ARTICLES

Sequential Pump-Dump Control of Photoisomerization Competing with Photodissociation of Optical Isomers

Kunihito Hoki,[†] Leticia González,[‡] Mohamed F. Shibl,[‡] and Yuichi Fujimura*[,†]

Department of Chemistry, Graduate School of Science, Tohoku University, Sendai, 980-8578, Japan, and Institut für Physikalische und Theoretische Chemie, Freie Universität Berlin, D-14195, Germany

Received: February 4, 2004; In Final Form: May 2, 2004

A sequential pump-dump control scenario for photoisomerization competing with direct photodissociation of a chiral molecule is derived by using a global optimization method. As an example, H_2POSD with axial chirality is considered. The first excited electronic state with n-σ^* electronic configuration is characterized by a repulsive potential that leads to P−S bond breaking. In this scenario, a first pump-dump sequence creates a nuclear wave packet having enough kinetic energy to cross the potential barrier in the ground state. This wave packet moves from one potential well corresponding to one of the optical isomers to the other in the electronic ground state. This transfer minimizes effects of the competing photodissociation. The second pump-dump sequence converts the wave packet into one having a small amount of kinetic energy via excitation to the first excited state. A stimulated Raman adiabatic passage (STIRAP) is applied to the same system for comparison. The yield of the photoisomerization obtained by using the STIRAP method is less than 0.1%, while that of using the sequential pump-dump pulse method is about 25%.

I. Introduction

Quantum control of nuclear wave packet manipulation guided by tailored laser pulses is now a major issue in femtosecond chemistry.[1−7] Photoisomerization of chiral molecules, i.e., chirality control, is a fascinating target in the quantum control of molecules,[8−17] since molecular chirality is important in not only synthetic chemistry but also biochemistry.[18]

We have proposed several kinds of control scenarios for molecular chirality.[19−29] These were applied to chiral molecules in a racemic mixture case as well as a pure state case. One of the scenarios is chiral control within its ground electronic state. This control is carried out by using picosecond IR laser pulses.[19] However, vibrational relaxation effects that compete with photoisomerization of chiral molecules occur and cannot be neglected in a picosecond time regime. Other control scenarios have been proposed in order to avoid such relaxation effects: a pump-dump laser control method via an electronic excited state by using a femtosecond laser pulse,[24] and a stimulated Raman adiabatic passage (STIRAP) by changing polarization direction adiabatically.[27] The latter method is applicable to a degenerated system in which the initial and final states have the same energy levels. Bound state models of simple chiral molecules, such as H_2POSH or H_2POSD, have been used to demonstrate effectiveness of the proposed scenarios. The dihedral angle, O−P−S−D, is the reaction coordinate of the molecular chirality.

We have found from ab initio MO calculations that the S_1 states of the chiral molecules H_2POSH, H_2POSD are characterized by a repulsive potential energy surface. The photodissociation process along the P−S bond is too fast to control the chirality by using an ordinary pump-dump method because nuclear wave packets excited by the pump pulse disappear from its Franck−Condon region within 5 fs.

In this paper, a new type of a pump-dump control method, consisting of two sequential pump-dump series of pulses, is proposed in order to control the photoisomerization of the chiral molecule H_2POSD with a repulsive potential in its electronic excited state (see Figure 1). This method has been derived by applying optimal control theory with an iteration algorithm.[30] The designed pulses consist of sequential pump-dump pulses as indicated by the arrows in Figure 1b. A nuclear wave packet with enough kinetic energy to cross the potential barrier in the electronic ground state is prepared via the excited state by the first pump-dump process (arrows 1). The wave packet runs from the potential well to the other one on the ground state. The wave packet having a large amount of kinetic energy is then transformed into one having a small amount of kinetic energy via an excited state by the second pump-dump process (arrows 2). As a result, a series of pump-dump pulses can reduce the period of the wave packet's stay in the dissociative excited state.

For comparison, chirality control by using the STIRAP method is presented. Since STIRAP does not create any population in an electronic excited state,[31] it was expected that this method would be effective regardless of whether the excited state has competing processes such as direct photodissociation. However, it is shown that the direct photodissociation process prevails over the isomerization process in the STIRAP procedure. This is because the direct photodissociation breaks down the adiabaticity of the STIRAP.

* Corresponding author.
[†] Tohoku University.
[‡] Freie Universität Berlin.

10.1021/jp0495038 CCC: $27.50
Published on Web 07/08/2004

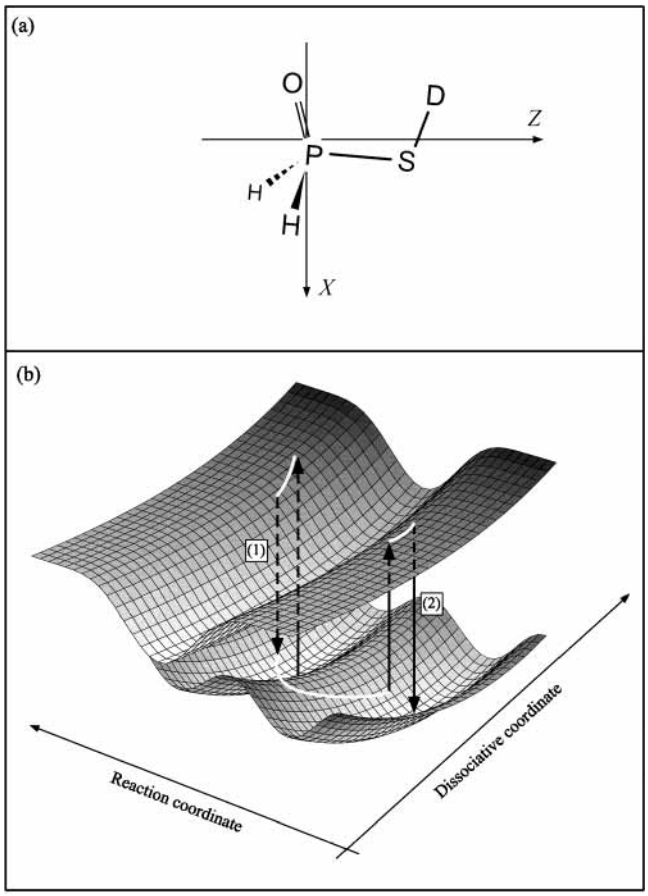

Figure 1. (a) Axial chiral molecule, H_2POSD, together with *X* and *Z* axes. The molecule has two stable configurations, in which the dihedral angle O−P−S−D is about −60 and 60 degrees. (b) Two-dimensional potential energy surfaces and a schematic picture of the sequential pump-dump scenario designed by the optimal control theory. The arrows denoted by (1) correspond to the first pump-dump process, and the arrows denoted by (2) correspond to the second pump-dump process.

In section II, a theoretical method for solving a two-dimensional model potential system of H_2POSD is presented taking into account the repulsive potential in S_1. In the two-dimensional model, the torsional degree of freedom is the reaction coordinate where the chirality changes, whereas the dissociation is the other degree of freedom. Fourier grid basis,[32] which is adapted to calculate two-dimensional nuclear wave functions, is shown. The explicit functional form of the Fourier grid basis and the relation between a continuous wave function and a series of discrete values are described in Appendix A. In section III, the electronic structure of H_2POSD calculated using the multiconfigurational complete active space self-consistent field (CASSCF) method[33] is described. Then a global optimization method is applied to photoisomerization of H_2POSD. An effective sequential pump-dump control scenario is derived from the analysis of the results obtained with the global optimization method.

II. Theoretical Methods

A. Representation of Nuclear Dynamics by Using an Adiabatic Basis Set. The time evolution of the molecular state $|\Psi(t)\rangle$ in the presence of laser pulses is described by the time-dependent Schrödinger equation

$$i\hbar \frac{\mathrm{d}}{\mathrm{d}t}|\Psi(t)\rangle = [\hat{H}_{\mathrm{M}} - \boldsymbol{\mu}\cdot\mathbf{E}(t)]|\Psi(t)\rangle = [\hat{T}_n + \hat{H}_{\mathrm{el}} - \boldsymbol{\mu}\cdot\mathbf{E}(t)]|\Psi(t)\rangle \quad (1)$$

where $\hat{H}_{\mathrm{M}}$ ($= \hat{T}_n + \hat{H}_{\mathrm{el}}$) is the molecular Hamiltonian that is expressed by the sum of the nuclear kinetic operator $\hat{T}_n$ and electronic Hamiltonian $\hat{H}_{\mathrm{el}}$, $\boldsymbol{\mu}$ is the dipole moment vector and $\mathbf{E}(t)$ is the electric field vector of the laser. Here, the molecule−electric field interaction is taken into account within the dipole approximation.

We expand the molecular state $|\Psi(t)\rangle$ in terms of the adiabatic basis set as

$$|\Psi(t)\rangle = \sum_n \int \mathrm{d}\mathbf{X}|n\mathbf{X}\rangle\chi_n(\mathbf{X},t) \quad (2)$$

where $|n\mathbf{X}\rangle = |n(\mathbf{X})\rangle|\mathbf{X}\rangle$ is the *n*th eigenvector of $\hat{H}_{\mathrm{el}}$ and simultaneously the eigenvector of position of nuclei $\hat{\mathbf{X}}$. Here, $|n(\mathbf{X})\rangle$ is an *n*th electronic state at specified nuclear positions $\mathbf{X}$, and $\chi_n(\mathbf{X},t)$ is the nuclear wave packet on the *n*th electronic state. Omitting effects of nonadiabatic couplings between electronic states, we can express eq 1 as a simultaneous partial differential equation for a set of nuclear wave packets $\chi_n(\mathbf{X},t)$, $n = 0, 1, 2, \ldots$ as

$$i\hbar \frac{\partial}{\partial t}\chi_n(\mathbf{X},t) = \int \mathrm{d}\mathbf{X}'\langle\mathbf{X}|\hat{T}_n|\mathbf{X}'\rangle\chi_n(\mathbf{X}',t) + V_n(\mathbf{X})\chi_n(\mathbf{X},t) - \sum_{n'}[\boldsymbol{\mu}_{nn'}(\mathbf{X})\cdot\mathbf{E}(t)]\chi_{n'}(\mathbf{X},t) \quad (3)$$

where $V_n(\mathbf{X})$ is the potential energy surface of the *n*th electronic state, and $\boldsymbol{\mu}_{nn'}(\mathbf{X})$ is the transition dipole moment between the *n*th and *n*′th electronic states.

For simplicity, consider an isomerization of a preoriented H_2POSD via the S_1 electronic state. In Figure 1a, the *Z*-axis is directed toward the center of mass of a rigid part, S−D, from that of $-POH_2$. The *X*-axis is parallel to the plane formed by the S, P, and O atoms. The potential energy surfaces are expressed in terms of two nuclear coordinates, ϕ and *r*. Here, ϕ, the reaction coordinate of the chirality change, is the dihedral angle of O−P−S−D defining molecular chirality (R) or (L). The coordinate *r* represents the distance between the center of mass of a rigid part, $-POH_2$, and that of −SD, and its potential in the S_1 state is repulsive.[34] Other degrees of freedom are considered uncoupled and therefore, frozen spectator modes. In passing, we note that the case of rotating fragments has been considered in ref 35.

Using these coordinates, the couplings between these nuclear motions vanish[34,36] and the matrix element of the nuclear kinetic operator is given by

$$\langle\mathbf{X}|\hat{T}_n|\mathbf{X}'\rangle = -\frac{\hbar^2}{2m_r}\frac{\partial^2\delta(r-r')}{\partial r^2} - \frac{\hbar^2}{2m_\phi}\frac{\partial^2\delta(\phi-\phi')}{\partial\phi^2} \quad (4)$$

where $n = 0$ or 1, and m_r and m_ϕ are the masses of the vibrational modes that move on the coordinates *r* and ϕ, respectively.

The molecular state $|\Psi(t)\rangle$ can then be expanded in terms of electronic states $|S_0\phi r\rangle$ and $|S_1\phi r\rangle$ with nuclear coordinates ϕ and *r* as

$$|\Psi(t)\rangle = \sum_{n=0,1}\int \mathrm{d}\phi \int \mathrm{d}r|S_n\phi r\rangle\chi_n(\phi,r,t) \quad (5)$$

The nuclear wave packet on S_0, $\chi_0(\phi,r,t)$, and that on the S_1 electronic state, $\chi_1(\phi,r,t)$, satisfy coupled time-propagation equations as

$$i\hbar \frac{\partial}{\partial t}\begin{pmatrix}\chi_0(\phi,r,t)\\ \chi_1(\phi,r,t)\end{pmatrix} = \begin{pmatrix}\hat{h}_0(\phi, r) & -\boldsymbol{\mu}_{01}(\phi,r)\cdot\mathbf{E}(t)\\ -\boldsymbol{\mu}_{10}(\phi,r)\cdot\mathbf{E}(t) & \hat{h}_1(\phi,r)\end{pmatrix}\begin{pmatrix}\chi_0(\phi,r,t)\\ \chi_1(\phi,r,t)\end{pmatrix} \quad (6)$$

where the vibrational Hamiltonian on each electronic state is given by

$$\hat{h}_n(\phi,r) = -\frac{\hbar^2}{2m_r}\frac{\partial^2}{\partial r^2} - \frac{\hbar^2}{2m_\phi}\frac{\partial^2}{\partial \phi^2} + V_n(\phi,r), (n = 0,1) \quad (7)$$

In eq 6, we omit the permanent dipole $\mu_{00}(\phi,r)$ and $\mu_{11}(\phi,r)$ since we are interested in quantum control by optical transitions between S_0 and S_1.

To numerically solve eq 6, we divide the Hamiltonian into kinetic and potential energy operators according to the split-operator + FFT (fast Fourier transform) scheme.[37−40] The potential couplings due to optical transitions are calculated using the Pauli matrix.[41]

B. Evaluation of a Two-Dimensional Eigenvalue Problem in Terms of a Grid Basis Set. We solve a two-dimensional eigenvalue problem on S_0 by means of the Fourier grid Hamiltonian technique,[32]

$$\hat{h}_0(\phi,r)\psi_{0j}(\phi,r) = E_{0j}\psi_{0j}(\phi,r) \quad (8)$$

where $\psi_{0j}(\phi,r)$ and E_{0j} are the jth nuclear wave function and eigenvalue on the S_0, respectively.

The two-dimensional wave function $\psi_{0j}(\phi,r)$ can be expanded by using a two-dimensional grid basis as (see Appendix A)

$$\psi_{0j}(\phi,r) = \sqrt{\Delta\phi}\sqrt{\Delta r}\sum_{n=0}^{N-1}\sum_{n'=0}^{N'-1}\psi_{0j}(\phi_n,r_{n'})\xi_n(\phi)\zeta_{n'}(r) \quad (9)$$

where $\phi_n = \phi_0 + n\Delta\phi$, $r_{n'} = r_0 + n'\Delta r$, $\Delta\phi = L/N$, and $\Delta r = L'/N'$. Here, the grid basis $\xi_n(\phi)$ and $\zeta_{n'}(r)$ are defined as (A.10) and (A.11), respectively

$$\xi_n(\phi) = \frac{1}{\sqrt{LN}}\sum_{m=m_s}^{m_e}\exp\left[2\pi i\left(\frac{\phi-\phi_0}{L} - \frac{n}{N}\right)m\right] \quad (10)$$

where $N = m_e - m_s + 1$, and

$$\zeta_{n'}(r) = \frac{1}{\sqrt{L'N'}}\sum_{m=m_s'}^{m_e'}\exp\left[2\pi i\left(\frac{r-r_0}{L'} - \frac{n'}{N'}\right)m\right] \quad (11)$$

where $N' = m_e' - m_s' + 1$.

The matrix element of $\hat{h}_0(\phi,r)$ is expressed in terms of the grid basis as

$$\begin{aligned}\{\hat{h}_0(\phi,r)\}_{nn'll'} &= \int_{\phi_0}^{\phi_N}\int_{r_0}^{r_N}\xi_n^*(\phi)\zeta_{n'}^*(r)\hat{h}_0(\phi,r)\xi_l(\phi)\zeta_{l'}(r)\,d\phi\,dr\\ &= \delta_{n'l'}\frac{\hbar^2}{2m_\phi}\frac{1}{N}\left(\frac{2\pi}{L}\right)^2\sum_{m=m_s'}^{m_e'}m^2\exp\left[2\pi i\frac{m(n-l)}{N}\right] + \\ &\quad \delta_{nl}\frac{\hbar^2}{2m_r}\frac{1}{N'}\left(\frac{2\pi}{L'}\right)^2\sum_{m=m_s'}^{m_e'}m^2\exp\left[2\pi i\frac{m(n'-l')}{N'}\right] + \\ &\quad \delta_{nl}\delta_{n'l'}V_0(\phi_n,r_{n'}) \quad (12)\end{aligned}$$

The two-dimensional eigenvalue problem on S_0, eq 8, is solved by diagonalizing the matrix $\{\hat{h}_0(\phi,r)\}_{nn'll'}$.

III. Results and Discussion

A. Electronic Structure Calculations. The potential energy surfaces were computed using the multiconfigurational complete active space self-consistent field (CASSCF) method,[33] implemented in the MOLCAS 4.3[42] quantum chemical software package. The initial geometry of H_2POSD was taken from ref 22. The active space consisted of 14 electrons correlated in 12 active orbitals, which include the lone pairs of oxygen and sulfur atoms, the σ, σ^* pairs of P−S and P═O bonds, and Rydberg orbitals. Within such active space, the lowest singlet state was found to be mainly a HOMO−LUMO transition corresponding to $n_S-\sigma^*_{P-S}$ excitation. The CASSCF calculations were made with the ANO-L basis set of the size (17s12p5d) primitives contracted to [5s4p3d] for the P and S atoms, (14s9p4d) contracted to [4s3p2d] for the O atom, and (8s4p) contracted to [3s2p] for the H atoms, summing in a total number of 114 contracted basis functions.

Figure 2 shows the potential energy surfaces of H_2POSD for S_0 and S_1 estimated at CASSCF (14, 12) level of theory. The potential energy surface in the ground electronic state has two stable configurations around $(\phi,r) = (-0.3\pi$ rad, 2.4 Å) and $(\phi,r) = (0.3\pi$ rad, 2.4 Å), which correspond to (L) and (R) forms of the enantiomer H_2POSD, respectively. There exists a transition state around $(\phi,r) = (0,$ 2.4 Å), and the energy difference between the transition state and the stable configuration is about 400 cm^{-1}. In contrast, the S_1 state does not have any stable configuration. This is because the main configuration of S_1 electronic state consists of n-σ^* excitation and it is repulsive along the P−S coordinate. A slice of the energy surface at a fixed r has a minimum at $\phi = 0$.

Figure 3 shows the calculated X, Y, and Z components of the transition dipole moment vector of H_2POSD. The absolute value of the transition dipole moment vector around the Franck−Condon region is ca. 0.05 D and, therefore, small compared with those in the case of electronic transitions between π and π^*, or between σ and σ^*. The X and Z components of the transition dipole moment vector are antisymmetric with respect to ϕ, whereas the Y component is symmetric.

B. Eigenvalue Problem in the Two-Dimensional Nuclear System. Figure 4 shows nuclear wave functions of the S_0 electronic state $\psi_{0j}^{\pm}(\phi,r)$, where $j = 0$, 1, 4, and 6. The signs + and − denote symmetric and antisymmetric with respect to the $X-Z$ plane, respectively. Here, the grid parameters $\phi_0 = -\pi$ rad, $\phi_N = \pi$ rad, $m_s = -32$, $m_e = 31$, $r_0 = 1.9$ Å, $r_N = 4.5$ Å, $m_s' = -128$, and $m_e' = 127$ are used. The masses are $m_r = 20.1$ amu and $m_\phi = 2.9$ Å^2 amu. To reduce computational time, we employed symmetric and antisymmetric grid bases for

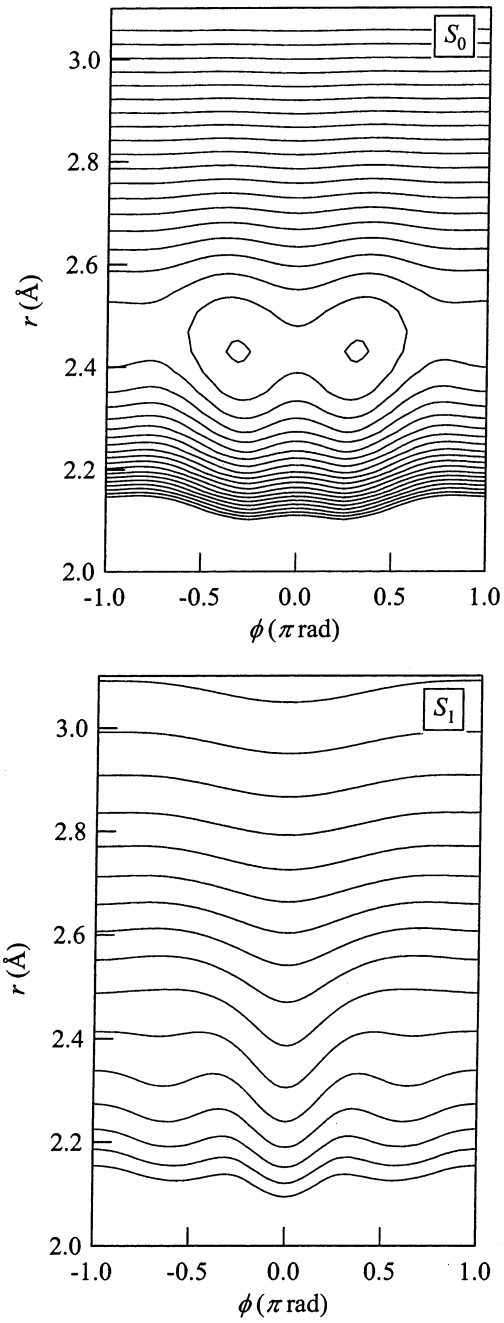

Figure 2. Contour plot of potential energy surfaces of S_0 and S_1 electronic states of H_2POSD. The nuclear coordinate ϕ represents an isomerization process, and r represents a dissociation process. The contour lines are drawn at regular intervals of 500 cm^{-1} or 2000 cm^{-1}.

ϕ, that is,

$$\xi_n^+(\phi) = \begin{cases} \xi_n(\phi) & (n = 0 \text{ or } N/2) \\ \frac{1}{\sqrt{2}}[\xi_n(\phi) + \xi_n(-\phi)] & (1 \le n \le N/2 - 1) \end{cases} \quad (13a)$$

and

$$\xi_n^-(\phi) = \frac{1}{\sqrt{2}}[\xi_n(\phi) - \xi_n(-\phi)] \quad (1 \le n \le N/2 - 1) \quad (13b)$$

respectively.

Localized vibrational states at each potential well in S_0 are formed by a superposition of the symmetric and asymmetric

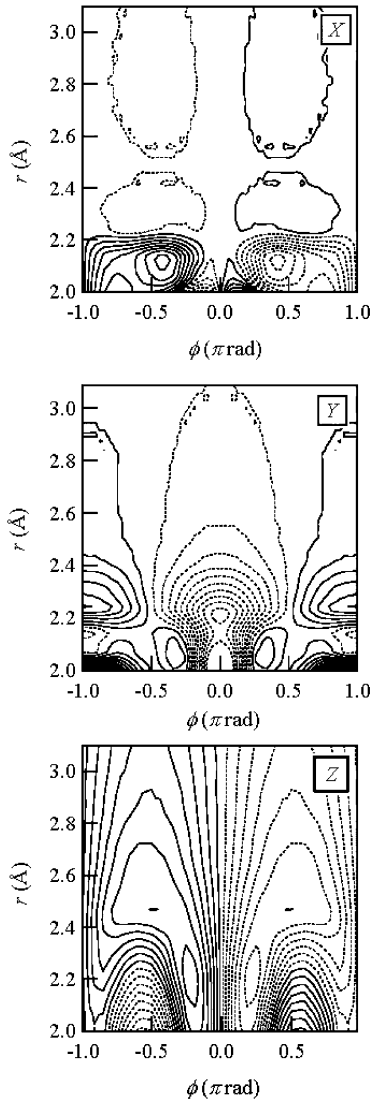

Figure 3. *X*, *Y*, and *Z* components of the transition dipole moment vector of H_2POSD. The solid contour lines are drawn at 0.01, 0.03, 0.05, etc. Debye. The dashed contour lines are drawn at −0.01, −0.03, −0.05, etc. Debye.

wave functions: for example, for the lowest vibrational state,

$$\psi_{00}^L(\phi,r) = \frac{1}{\sqrt{2}}[\psi_{00}^+(\phi,r) + \psi_{00}^-(\phi,r)] \quad (14a)$$

$$\psi_{00}^R(\phi,r) = \frac{1}{\sqrt{2}}[\psi_{00}^+(\phi,r) - \psi_{00}^-(\phi,r)] \quad (14b)$$

The periods of tunneling, L → R → L, are about 1700 ps for $j = 0$, 50 ps for $j = 1$, 47 ps for $j = 4$, and 17 ps for $j = 6$. Other localized states have shorter periods, e.g., 3.7 ps for $j = 2$.

C. Photoisomerization by STIRAP. Before showing results obtained by using optimal control theory, we present results obtained by using a STIRAP method that has been developed by us.[27] Consider the photoisomerization from the L- form to the R- form of H_2POSD. The chirality change from (L) to (R) is achieved by adiabatically changing the polarization direction of the electric field. The electric field is expressed as

$$\mathbf{E}(t) = \mathbf{A}(t)\cos(\omega t) \quad (15)$$

where $\mathbf{A}(t)$ denotes the time-dependent amplitude and the time-

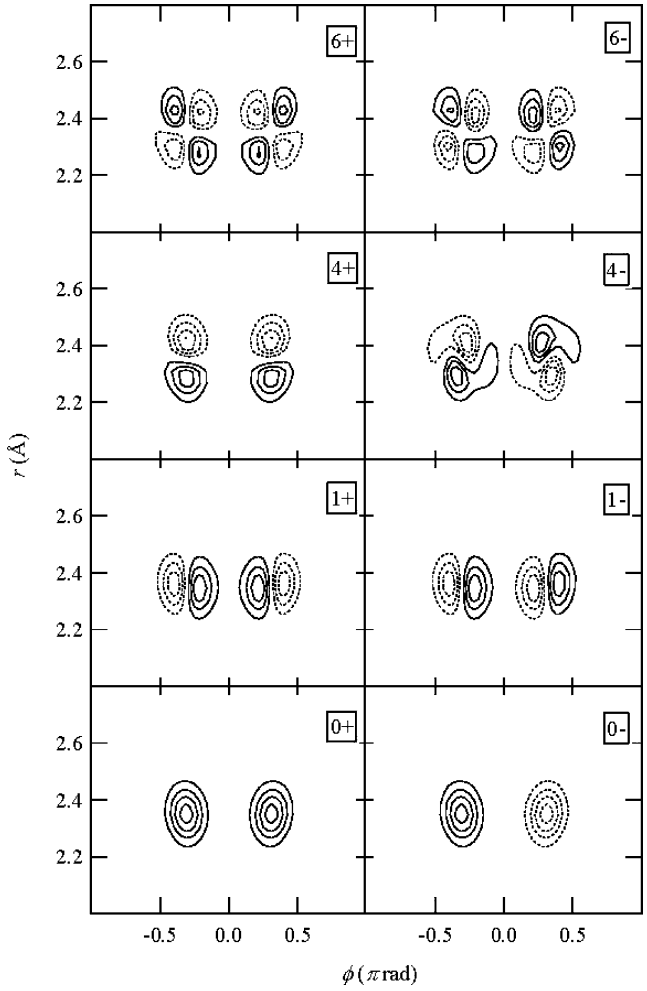

Figure 4. Nuclear wave functions $\psi^{\pm}_{0j}(\phi,r)$. Here, the signs + and − denote symmetry with respect to the $X-Z$ plane.

dependent polarization direction of the electric field. The direction of $\mathbf{A}(t)$ is chosen to sweep from an angle that is orthogonal to $\boldsymbol{\mu}^{L}_{00,1\nu}$ to an angle that is orthogonal to $\boldsymbol{\mu}^{R}_{00,1\nu}$. Here, $\boldsymbol{\mu}^{L}_{00,1\nu}$ and $\boldsymbol{\mu}^{R}_{00,1\nu}$ are the matrix elements of the transition moment vector between the lowest localized state in the ground state and a vibronic state in the S_1 electronic state as

$$\boldsymbol{\mu}^{L}_{00,1\nu} = \int \mathrm{d}\phi \int \mathrm{d}r \psi^{L}_{00}(\phi,r)^{*}\boldsymbol{\mu}_{01}(\phi,r)\psi_{1\nu}(\phi,r) \quad (16)$$

The direction of $\mathbf{A}(t)$ at $t = t_0$ and that at $t = t_f$ satisfy the following conditions:

$$\mathbf{A}(t_0)\cdot\boldsymbol{\mu}^{R}_{00,1\nu} \neq 0 \text{ and } \mathbf{A}(t_0)\cdot\boldsymbol{\mu}^{L}_{00,1\nu} = 0 \quad (17a)$$

and

$$\mathbf{A}(t_f)\cdot\boldsymbol{\mu}^{L}_{00,1\nu} \neq 0 \text{ and } \mathbf{A}(t_f)\cdot\boldsymbol{\mu}^{R}_{00,1\nu} = 0 \quad (17b)$$

We set the initial state as an (L)-molecule $|0L\rangle = \int \mathrm{d}r \int \mathrm{d}\phi |S_0\phi r\rangle \psi^{L}_{00}(\phi,r)$. The $\mathbf{A}(t)$ was set to be

$$\mathbf{A}(t) = E_0[\mathbf{e}_X \cos\theta(t) + \mathbf{e}_Y \sin\theta(t)] \quad (18)$$

where $E_0 = 5.0 \times 10^9$ *V/m* and

$$\theta(t) = 0.65\pi - 0.30\pi \sin^2\left(\frac{\pi t}{40}\right) \quad (19)$$

in ps units of *t*.

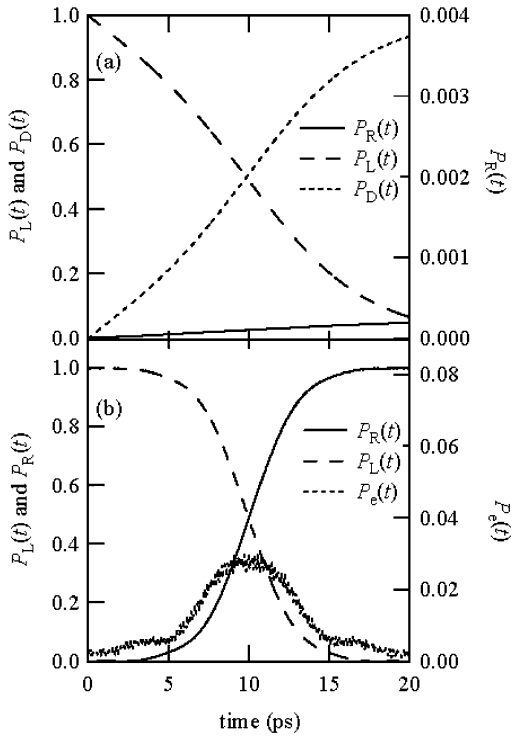

Figure 5. Time propagation of populations by STIRAP. Panel (a) shows the results in the case in which the dissociation process is taken into account. $P_R(t)$ and $P_L(t)$ are populations localizing at right and left potential wells in the S_0 state, respectively. $P_D(t)$ is the sum of the population in the electric excited state and that absorbed by the boundary, and it directly corresponds to the probability of dissociation. Panel (b) shows the results in the case in which the kinetic energy of the nuclear motion along *r* is omitted to prohibit the dissociation process. $P_e(t)$ is a population in the S_1 state.

The frequency of the field was set to be $\omega = 47818$ cm^{-1}, which corresponds to the resonance frequency evaluated at fixed nuclear distances.

Figure 5a shows results obtained by using the STIRAP method. The photoisomerization yield is only 0.02%, and the photodissociation probability is 0.93 at $t = 20$ ps. These results mean that the isomerization and dissociation processes are competing processes. STIRAP does not create any population in the intermediate state, if the adiabatic condition is satisfied. However, the dissociation process causes the breakdown of the adiabatic condition, and most of the wave packet created in the S_1 state goes into the direct photodissociation channel. The breakdown of adiabatic passage for STIRAP involving a resonant intermediate state has theoretically been treated in ref 43. To determine the origin of the breakdown of adiabatic condition, we applied the STIRAP method to a model system of H_2POSD in which the nuclear motion along *r* is fixed at $r = 2.35$ Å to prevent a direct photodissociation process. The results are shown in Figure 5b. The same electric field as that used in Figure 5a was applied. The photoisomerization process from (L) to (R) is accomplished with about 100% yield.

We note that an attempt of making the passage time shorter to suppress the dissociation process also causes the breakdown of the STIRAP. In the case of fixed motion along *r*, the passage time of 20 ps is the threshold to obtain the yield of almost 100%. The applicability of STIRAP to systems with continuum or *N*-level has been studied using a simple model.[44,45] On the other hand, the result shown in Figure 5 is an example that shows limit of STIRAP via continuum.[46]

D. Photoisomerization by an Optimal Control. A monotonically convergent iteration algorithm developed by Zhu and

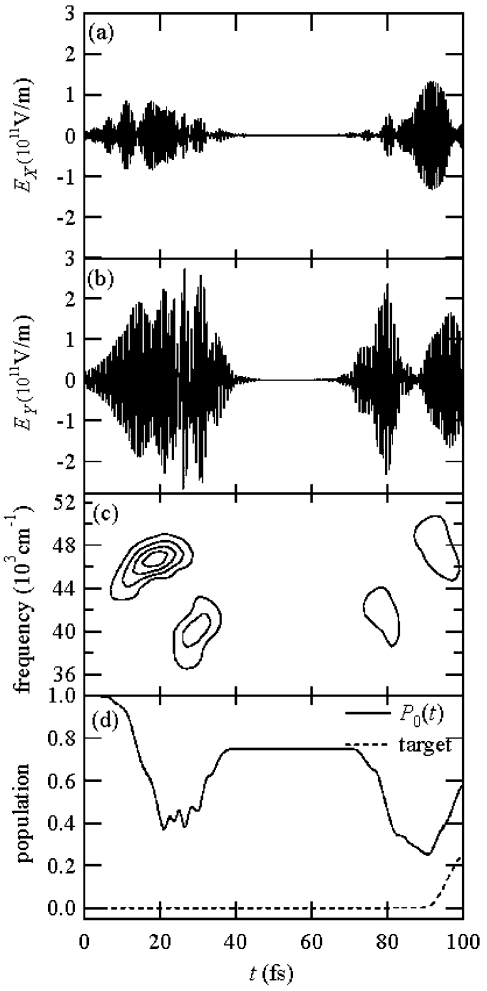

Figure 6. Calculated optimal pulse and time propagation of populations for the control of isomerization in the presence of the dissociation process. The panels (a) and (b) denote the *X* and *Y* components of the electric field vector, respectively. The panel (c) shows a time-frequency resolved spectrum of the electric field vector. The fwhm of the window function, which corresponds to the time resolution, is chosen as 10 fs. The solid line in panel (d) denotes time propagation of the population in the electronic ground state S_0, $P_0(t)$ and the dashed line denotes that of the expectation value of the target operator $\hat{W}_R$ under the optimal pulse condition.

Rabitz was used to derive optimal electric fields of laser pulses.[30] The algorithm converges monotonically and quadratically in terms of the neighboring field deviations, if the expectation value of the target operator $\hat{W}$ is positive definite. In their original formulation in ref 30, the electric field function and the dipole moment are not vectors. The convergence property is still valid even if we substitute the dipole interaction $-\boldsymbol{\mu}\cdot\mathbf{E}(t)$ for $-\mu E(t)$.

We set the initial state as $|0L\rangle$ and the target operator $\hat{W}_R = |0R\rangle\langle 0R| + |1R\rangle\langle 1R| + |4R\rangle\langle 4R| + |6R\rangle\langle 6R|$, in which numbers denote vibrational quantum numbers in the ground electronic state of an R-form H_2POSD. We set the final time $t_f = 100$ fs and two components of the electric field vector $E_X(t)$ and $E_Y(t)$. The grid basis for ϕ and that for r were taken to be the same as those used in calculating wave functions, and the step of the time propagation is $\Delta t = 0.005$ fs. Since the potential energy surface on S_1 is repulsive, we used an absorbing boundary in the region of 3.9 Å $< r <$ 4.5 Å. To carry out the iteration algorithm consisting of successive forward and backward propagations, the absorbed amplitudes were stored every 5 fs.

Figures 6a and b show the *X* and *Y* components of the electric field obtained by the optimal control method, respectively. The electric field vector, which selectively controls the preoriented molecular chirality in the pure state picture, is elliptically polarized, and the direction of polarization changes with passage of time. The control electric field consists of two sets of pump-dump pulses. From 5 to 40 fs, the first pump and dump pulses are applied, transferring populations between the S_0 and S_1 electronic states. The second pump and dump pulses operate from 70 to 100 fs, and the target state is formed by the last dump process.

Figure 6c shows the time-frequency resolved spectrum used to analyze the pump and dump processes and to clarify the time-dependent phase of the electric field. The spectrum was calculated by using Parzen window function.[47] The peaks of the four pulses are well separated from each other. This means that the electric field vector consists of four separate pulses rather than two Raman pulses or an intra-pump-dump pulse.[48] Furthermore, each pulse is chirped for timing of excitation or deexcitation of wave packet components.[49,50] It is interesting to compare our results with results reported by Shen et al.[51] They have used penalty methods coupled with unitary exponential operator methods to optimize envelope functions of pump and dump pulses in a three-level-system. In contrast to our result, their result has simple envelope functions described by trigonometric functions.

Figure 6d shows the time-dependent population in the electronic ground state S_0, and the expectation value of the target operator $\hat{W}_R$. After the first pump-dump process, ca. 0.25 of probability is left in the S_1 electronic state, and all of it dissociates. Similarly, after the second pump-dump process, ca. 0.17 of probability dissociates. After the second pump-dump process, the expectation value of the target operator $\hat{W}_L = |0L\rangle\langle 0L| + |1L\rangle\langle 1L| + |4L\rangle\langle 4L| + |6L\rangle\langle 6L|$ is 0.25, whereas that of the other operator is 0.02. The amount of the residue, 0.31 remains on vibrationally excited states of S_0.

We should note that H_2POSD is ionized by electric fields of the order of 10^{11} V/m, shown in Figure 6a and b; however, for the sake of simplicity, ionization processes were omitted in the treatment. The value of the Keldysh parameter, $\gamma = \omega_L\sqrt{2I_p}/f(t)$, was estimated to be 0.4, where the maximum field amplitude was used for $f(t)$, the wavelength of the electric field ω_L was assumed to be 200 nm, and the ionization potential of the molecule I_p was estimated to be 10 eV. Since the parameter is less than 1, H_2POSD is ionized due to tunnel ionization processes. Molecular dissociation and ionization dynamics in intense laser fields are now one of the hot topics in chemical reaction studies.[52] Several types of the theoretical approaches, such as the time-dependent adiabatic state approach, have been proposed.[53] It is quite interesting to extend the optimal control method used here to molecular systems characterized by both dissociation and ionization paths. To deal with the system more closely, it will be required to handle changes of potential surfaces due to the ionization process.

Figure 7 shows the temporal evolution of nuclear wave packets on the S_0 (lower panels) and S_1 (upper panels) two-dimensional potential surfaces. From this figure, we can see how the pump-dump control pulses handle the wave packets to prevent direct dissociation in the electronic excited state. At $t = 20$ fs, a component of the wave packet is excited in the S_1 electronic state, where it runs in a positive direction for both ϕ and r because of the slope of the S_1 potential energy surface. Before the excited component acquires a level of kinetic energy sufficient to dissociate the P−S bond on the S_1 electronic surface, the control pulse transfers the component to the S_0

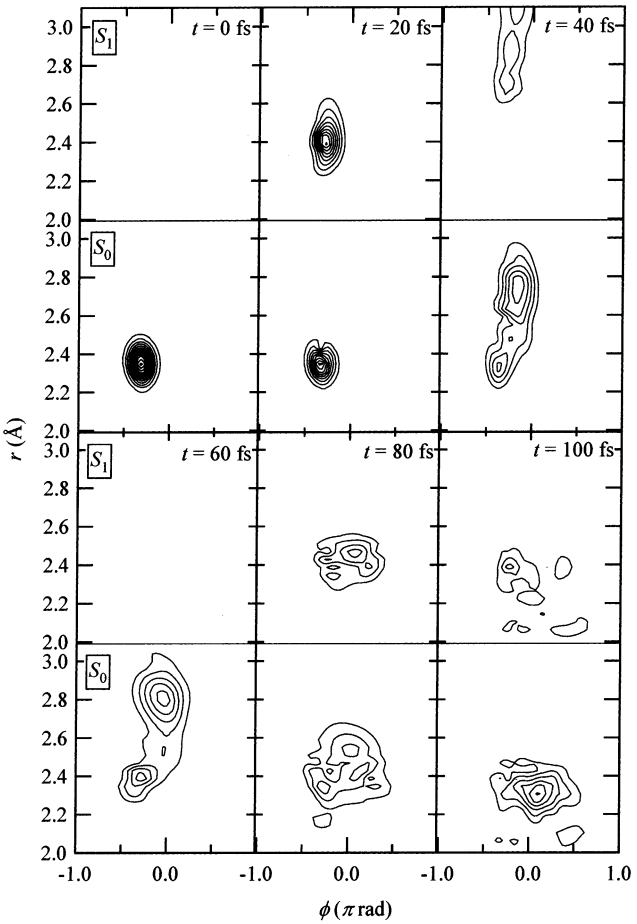

Figure 7. Time propagation of nuclear wave packets under the optimal pulse condition. Each figure corresponds to the contour plot of the wave packet at 0, 20, 40, 60, 80, and 100 fs in the S_1 (up) and S_0 (down).

electronic surface within 10 fs. After the first pump-dump process, at $t = 40$ fs, a component of the wave packet is created on the S_0 electronic potential surface with larger vibrational energy than that of the potential barrier at $\phi = 0$. On the other hand, a part of the component of the wave packet still remains on the repulsive potential surface, and this dissociation process has a probability of 0.25. When the main component of the wave packet in the S_0 electronic state crosses the potential barrier, the second pump-dump pulses are irradiated to obtain a wave packet in the S_0 electronic state with a low level of vibrational energy, which is a stable configuration of the R-enantiomer. In the second set of the pump-dump processes, the excited component is also quickly transferred to the S_0 electronic state to suppress the dissociation process.

So far, we have restricted ourselves to photoisomerization of a chiral molecule in the pure state case. We now present a rough treatment of a photoisomerization in a mixed case. This consists of using the electric fields in the pure state case described above. For simplicity, it is assumed that there are no dephasing processes.

It has been shown that the designed optimal electric field vector $\mathbf{E}(t)$ produces 25% of R-form and 2% of L-form from the initial state $|0\mathrm{L}\rangle$ in the pure state case. This means that $\langle 0\mathrm{L}|\hat{U}(t_0,t_f,\mathbf{E})\hat{W}_\mathrm{R}\hat{U}(t_f,t_0,\mathbf{E})|0\mathrm{L}\rangle \cong 0.25$ and $\langle 0\mathrm{L}|\hat{U}(t_0,t_f,\mathbf{E})\hat{W}_\mathrm{L}\hat{U}(t_f,t_0,\mathbf{E})|0\mathrm{L}\rangle \cong 0.02$, where $U(t,t',E)$ is the time propagation operator that satisfies

$$i\hbar\frac{\partial}{\partial t}\hat{U}(t,t',\mathbf{E}) = [\hat{H}_M - \boldsymbol{\mu}\cdot\mathbf{E}(t)]\hat{U}(t,t',\mathbf{E}) \qquad (20)$$

with boundary condition $\hat{U}(t,t,\mathbf{E}) = 1$. On the other hand, the electric field vector produces 2% of R-form and 7% of L-form from the other initial state $|0\mathrm{R}\rangle$. That is, $\langle 0R|\hat{U}(t_0,t_f,\mathbf{E})\hat{W}_\mathrm{R}\hat{U}(t_f,t_0,\mathbf{E})|0\mathrm{R}\rangle \cong 0.02$ and $\langle 0\mathrm{R}|\hat{U}(t_0,t_f,\mathbf{E})\hat{W}_\mathrm{L}\hat{U}(t_f,t_0,\mathbf{E})|0\mathrm{R}\rangle \cong 0.07$. If we set an initial density matrix in low-temperature limits as $\rho(t_0) = (1/2)[|0\mathrm{L}\rangle\langle 0\mathrm{L}| + |0\mathrm{R}\rangle\langle 0\mathrm{R}|]$, the populations of (R) and (L) molecules are given as $\mathrm{Tr}[U(t_f,t_0,E)\rho(t_0)U(t_0,t_f,E)\hat{W}_\mathrm{R}] \cong 0.14$ and $\mathrm{Tr}[U(t_f,t_0,E)\rho(t_0)U(t_0,t_f,E)\hat{W}_\mathrm{L}] \cong 0.05$, respectively. It should be noted that (R) molecules from the preoriented racemic mixture were prepared by using an asymmetric interaction consisting of a symmetric interaction induced by $E_Y(t)$ and an antisymmetric interaction induced by $E_X(t)$ that were determined by the optimal control procedure in the pure state case. On the other hand, the reflected electric field vector components, $-E_Y(t)$ and $E_X(t)$, were adopted to select (L) molecules.

For further study of wave packet control in a mixed state with competing processes in an electronic excited state, electric field vector $\mathbf{E}(t)$ should be optimized in density matrix formalism.[54−57] The optimal field vector is designed to maximize the population of (R) molecules with the other initial state $|0\mathrm{R}\rangle$ as well as the initial state $|0\mathrm{L}\rangle$. On the other hand, a selective extraction method in the mixed state is worth applying to a dissipating system.[34] In this case, the yield is limited to 50%. However, since this scheme makes use of the unfavorable dissociation process actively, this scheme is an attractive method if competing dissociative processes are strong.

It would be interesting to apply the designed sequential pump-dump pulses to other photoisomerization processes competing with photodissociation or other photophysical or photochemical processes occurring in an electronic excited state.[58] Such systems can be seen in many organic compounds such as metal complexes or biomolecules.[59] However, it should be noted that the present control method should be applied to systems that have a smooth ground potential energy surface in order to keep the ground-state wave packet localized.

In summary, we have presented an effective scenario of quantum control of photoisomerization of a chiral molecule competing with direct photodissociation. Photoisomerization of a molecule with axial chirality, H_2POSD, was considered. The optimal pulses consist of sequential pump-dump pulses that minimize effects of the competing direct photodissociation. To demonstrate the effectiveness of the sequential pump-dump pulse method, a STIRAP method was applied to the same reaction system. The photoisomerization yield obtained by using the STIRAP method was less than 0.1%, while that obtained by using the sequential pump-dump pulse method was 25%.

Because of the forbidden transition between the ground and the first excited state of H_2POSD, electric fields of an order of 10^{11} V/m were obtained by using the optimal control method. This means that ionization processes make a significant contribution as well as the P−S bond breaking in the photoisomerization. It will be the next step to develop control scenarios of molecular processes including two open channels of dissociation and ionization.

Acknowledgment. This work was partly supported by Grants-in-Aid for Scientific Research from the Ministry of Education, Science, Sports, Culture and Technology, Japan (No. 1555002), a Grant-in Aid for Scientific Research on Priority Areas, "Control of Molecules in Intense Laser Fields" (No. 419), and the DFG, Project Ma 515/18-3.

Appendix A. Evaluation of a Two-Dimensional Eigenvalue Problem in Terms of Grid Basis Set

Consider a two-dimensional eigenvalue problem, eq 8

$$\hat{h}_0(\phi,r)\psi_{0j}(\phi,r) = E_{0j}\psi_{0j}(\phi,r) \tag{A.1}$$

where $\psi_{0j}(\phi,r)$ and E_{0j} are jth nuclear wave function and eigenvalue of S_0, respectively.

To evaluate eq A.1 by means of the Fourier grid Hamiltonian technique, for simplicity, consider a one-dimensional grid basis before treating a two-dimensional case. Here, the Fourier grid basis $\xi_n(x)$ is given under an approximation by means of limited Fourier expansion. Similarly, the relation between a continuous function $f(x)$ and a series of discrete values $f(x_n)$ is given by using the basis $\xi_n(x)$.

Since it is difficult to treat a variable from minus infinity to positive infinity by using restricted computer resources, we set all of the one-dimensional functions of x, $f(x)$, wave functions, or molecular potential to a boundary condition, $f(x) = f(x + L)$. Furthermore, the function $f(x)$ is assumed to be formed from a limited Fourier components as

$$f(x) = \frac{1}{\sqrt{L}} \sum_{m=m_s}^{m_e} \tilde{f}_m \exp\left(2\pi i \frac{x - x_0}{L} m\right) \tag{A.2}$$

Here, an inner product of such functions $f_1(x)$ and $f_2(x)$ is written as

$$\int_{x_0}^{x_0+L} f_1^*(x) f_2(x)\, dx = \Delta x \sum_{n=0}^{N-1} f_1(x_n) f_2(x_n) \tag{A.3}$$

where the number of Fourier components is $N = m_e - m_s + 1$, $\Delta x = L/N$, and $x_n = x_0 + n\,\Delta x$. The one-dimensional grid basis is written as

$$\xi_n(x) = \frac{1}{\sqrt{LN}} \sum_{m=m_s}^{m_e} \exp\left[2\pi i\left(\frac{x - x_0}{L} - \frac{n}{N}\right)m\right] \tag{A.4}$$

It should be noted that the shape of the function $\xi_n(x)$ is localized around $x = x_n$ with width Δx. It is confirmed that the function $\xi_n(x)$ satisfies the essential properties as a grid basis,

$$f(x) = \sqrt{\Delta x} \sum_{n=0}^{N-1} f(x_n)\xi_n(x) \tag{A.5}$$

for all functions $f(x)$ that satisfy condition (A.2), and

$$\int_{x_0}^{x_N} \xi_n^*(x)\xi_l(x)\, dx = \delta_{nl} \tag{A.6}$$

where $0 \le n,l \le N - 1$. By using this grid basis, we obtain a matrix element of a function $f(x)$ as

$$\int_{x_0}^{x_N} \xi_n^*(x) f(x)\, \xi_l(x)\, dx = f(x_n)\delta_{nl} \tag{A.7}$$

and that of the second differential operator as

$$\int_{x_0}^{x_N} \xi_n^*(x) \frac{d^2}{dx^2}\xi_l(x)\, dx = -\frac{1}{N}\left(\frac{2\pi}{L}\right) \sum_{m=m_s}^{m_e} m^2 \exp\left[2\pi i \frac{m(n-1)}{N}\right] \tag{A.8}$$

The right-hand side of eq A.8 can be evaluated by using an FFT program package, and the value is real if we set appropriate parameters to m_s and m_e, e.g., $m_s = -N/2$ and $m_e = N/2-1$ with an even integer N.

Two-dimensional wave function $\psi_{0j}(\phi,r)$ can now be expanded by using a two-dimensional grid basis in a manner similar to that in the one-dimensional case as

$$\psi_{0j}(\phi,r) = \sqrt{\Delta\phi}\,\sqrt{\Delta r} \sum_{n=0}^{N-1} \sum_{n'=0}^{N'-1} \psi_{0j}(\phi_n,r_{n'})\xi_n(\phi)\zeta_{n'}(r) \tag{A.9}$$

where $\phi_n = \phi_0 + n\Delta\phi$, $r_{n'} = r_0 + n\Delta r$, $\Delta\phi = L/N$, and $\Delta r = L'/N'$. Here, the grid bases $\xi_n(\phi)$ and $\zeta_{n'}(r)$ are defined as

$$\xi_n(\phi) = \frac{1}{LN} \sum_{m=m_s}^{m_e} \exp\left[2\pi i\left(\frac{\phi - \phi_0}{L} - \frac{n}{N}\right)m\right] \tag{A.10}$$

where $N = m_e - m_s + 1$ and

$$\zeta_{n'}(r) = \frac{1}{\sqrt{L'N'}} \sum_{m=m_s}^{m_e} \exp\left[2\pi i\left(\frac{r - r_0}{L'} - \frac{n'}{N'}\right)m'\right] \tag{A.11}$$

respectively. Here $N' = m_e' - m_s' + 1$, respectively. Thus, the matrix element of $\hat{h}_0(\phi,r)$ can be represented by the grid basis as

$$\begin{aligned}\{\hat{h}_0(\phi,r)\}_{nn'll'} &= \int_{\phi_0}^{\phi_N}\int_{r_0}^{r_N} \xi_n^*(\phi)\zeta_{n'}^*(r)\hat{h}_0(\phi,r)\xi_l(\phi)\zeta_{l'}(r)\, d\phi\, dr \\ &= \delta_{n'l'}\frac{\hbar^2}{2m_\phi}\frac{1}{N}\left(\frac{2\pi}{L}\right)^2 \sum_{m=m_s'}^{m_e'} m^2 \exp\left[2\pi i \frac{m(n-l)}{N}\right] + \\ &\quad \delta_{nl}\frac{\hbar^2}{2m_r}\frac{1}{N'}\left(\frac{2\pi}{L'}\right)^2 \sum_{m=m_s'}^{m_e'} m^2 \exp\left[2\pi i \frac{m(n'-l')}{N'}\right] + \\ &\quad \delta_{nl}\delta_{n'l'}V_0(\phi_n,r_n')\end{aligned} \tag{A.12}$$

References and Notes

(1) Tannor, D. J.; Rice, S. A. *J. Chem. Phys.* **1985**, *83*, 5013.
(2) Kohler, B.; Krause, J. L.; Raksi, F.; Wilson, K. R.; Yakovlev, V. V.; Whitnell, R. M.; Yan, Y. J. *Acc. Chem. Res.* **1995**, *28*, 133.
(3) Zewail, A. H. *Adv. Chem. Phys.* **1997**, *101*, 3.
(4) Assion, A.; Baumert, T.; Bergt, M.; Brixner, T., Kiefer, B.; Seyfried, V.; Strehle, M.; Gerber, G. *Science* **1998**, *282*, 919.
(5) Gordon, R. A.; Fujimura, Y. *Encyclopedia of Physical Science and Technology*; Academic Press: San Diego, 2002; p 207.
(6) Brixner, T.; Damrauer, N. H.; Krampert, G.; Niklaus, P.; Gerber, G. *J. Mod. Opt.* **2003**, *50*, 539.
(7) Daniel, C.; Full, J.; González, L.; Lupulescu, C.; Manz, J.; Merli, A.; Vajda, S.; Wöste, L. *Science* **2003**, *299*, 536.
(8) Inoue, Y. *Chem. Rev.* **1992**, *92*, 741.
(9) Avalos, B. M.; Babiano, R.; Cintas, P.; Jimenez, J.; Palacios, J. C.; Barron, L. D. *Chem. Rev.* **1998**, *98*, 2391.
(10) Shapiro, M.; Brumer, P. *J. Chem. Phys.* **1991**, *95*, 8658.
(11) Cina, J. A.; Harris, R. A. *J. Chem. Phys.* **1994**, *100*, 253.
(12) Shao, J.; Hänggi, P. J. *Chem. Phys.* **1997**, *107*, 9935.
(13) Salam, A.; Meath, W. J. *J. Chem. Phys.* **1997**, *106*, 7865.
(14) Salam, A.; Meath, W. J. *Chem. Phys.* **1998**, *228*, 115.
(15) Shapiro, M.; Frishman, E.; Brumer, P. *Phys. Rev. Lett.* **2000**, *84*, 1669.
(16) Bychkov, S. S.; Grishanin, B. A.; Zadkov, V. N.; Takahashi, H. *J. Raman Spectrosc.* **2002**, *33*, 962.
(17) Frishman, E.; Shapiro, M.; Gerbasi, D.; Brumer, P. *J. Chem. Phys.* **2003**, *119*, 7237.
(18) Noyori, R. *Angew. Chem., Int. Ed.* (Nobel Lecture) **2002**, *41*, 2008.
(19) Fujimura, Y.; González, L.; Hoki, K.; Manz, J.; Ohtsuki, Y. *Chem. Phys. Lett.* **1999**, *306*, 1; *Corrigendum* **1999**, *310*, 578.
(20) Fujimura, Y.; González, L.; Hoki, K.; Kröner, D.; Manz, J.; Ohtsuki, Y. *Angew. Chem., Int. Ed.* **2000**, *39*, 4586.

(21) Hoki, K.; Ohtsuki, Y.; Fujimura, Y. *J. Chem. Phys*. **2001**, *114*, 1575.
(22) González, L.; Kröner, D.; Solá, I. R. *J. Chem. Phys.* **2001**, *115*, 2519.
(23) Hoki, K.; Fujimura, Y. *Laser control and manipulation of molecules*; Bandrauk, A. D.; Fujimura, Y.; Gordon, R. J., Eds.; American Chemical Society: Washington DC, 2002; p 32.
(24) Hoki, K.; González, L.; Fujimura, Y. *J. Chem. Phys.* **2002**, *116*, 2433.
(25) Hoki, K.; González, L.; Fujimura, Y. *J. Chem. Phys.* **2002**, *116*, 8799.
(26) Umeda, H.; Takagi, M.; Yamada, S.; Koseki, S.; Fujimura, Y. *J. Am. Chem. Soc*. **2002**, *124*, 9265.
(27) Ohta, Y.; Hoki, K.; Fujimura, Y. *J. Chem. Phys*. **2002**, *116*, 7509.
(28) Kröner, D.; González, L. *Phys. Chem. Chem. Phys*. **2003**, *5*, 3933.
(29) Kröner, D.; Shibl, M. F.; González, L. *Chem. Phys. Lett.* **2003**, *372*, 242.
(30) Zhu, W.; Rabitz, H. *J. Chem. Phys*. **1998**, *109*, 385.
(31) Bergmann, K.; Theuer, H.; Shore, B. W. *Rev. Mod. Phys*. **1998**, *70*, 1003.
(32) Marston, C. C.; Balint-Kurti, G. G. *J. Chem. Phys*. **1989**, *91*, 3571.
(33) Roos, B. O.; Taylor, P. R.; Siegbahn, P. E. M. *Chem. Phys*. **1980**, *48*, 157.
(34) González, L.; Manz, J; Schmidt, B.; Shibl, M. F., to be published.
(35) Hoki, K.; Kröner, D.; Manz, J. *Chem. Phys*. **2001**, *267*, 59.
(36) Manz, J. *Mol. Phys*. **1971**, *21*, 641.
(37) Feit, M. D.; Fleck, J. A. *J. Chem. Phys.***1983**, *78*, 301.
(38) Kono, H.; Lin, S. H. *J. Chem. Phys.* **1986**, *84*, 1071.
(39) Bandrauk, A. D.; Shen, H. *J. Chem. Phys.* **1993**, *99*, 1185.
(40) Alvarellos, J.; Metiu, H. *J. Chem. Phys*. **1988**, *88*, 4957.
(41) Gross, P.; Neuhauser, D.; Rabitz, H. *J. Chem. Phys.* **1992**, *96*, 2834.
(42) Andersson, K.; Blomberg, M. R. A.; Fulscher, M. P.; Karlstrom, G.; Lindh, R.; Malmqvist, P.-A.; Neogrady, P.; Olsen, J.; Roos, B. O.; Sadlej, A. J.; Schutz, M.; Seijo, L.; Serrano-Andres, L.; Siegbahn, P. E. M.; Widmark, P.-O. MOLCAS Ver. 4. Department of Theoretical Chemistry, Chem. Cent., University of Lund, P. O. Box 124, S-22100 Lund, 1997.
(43) Kobrak, M. N.; Rice, S. A. *Phys. Rev. A* **1998**, *57*, 1158.
(44) Carroll, C. E.; Hioe, F. T. *Phys. Rev. Lett.* **1992**, *68*, 3523.
(45) Malinovsky, V. S.; Tannor, D. J. *Phys. Rev. A* **1997**, *56*, 4929.
(46) Nakajima, T.; Zhang, J.; Elk, M.; Lambropoulos, *P. Phys. Rev. A* **1994**, *50*, R913.
(47) Flannery, B. P.; Teukolsky, S. A.; Vetterling, W. T. *Numerical Recipes in C: The Art Of Scientific Computing*; Press, W. H., Ed.; Cambridge University Press: New York, 1988.
(48) Bardeen, C. J.; Wang, Q.; Shank, C. V. *Phys. Rev. Lett.* **1995**, *75*, 3410.
(49) Chelkowski, S.; Bandrauk, A. D.; Corkum, P. B. *Phys. Rev. Lett.* **1990**, *65*, 2355.
(50) *Quantum Control: mathematical and numerical challenges*; Bandrauk, A. D., Delfour, M. C., Le Bris, C., Eds.; CRM Proceedings Lecture Notes Series, AMS Publications: Providence RI.
(51) Shen, H.; Dussault, J.-P.; Bandrauk, A. D. *Chem. Phys. Lett*. **1994**, *221*, 498.
(52) Yamanouchi, K. *Science* **2002**, *295*, 1659.
(53) Sato, Y.; Kono, H.; Koseki, S.; Fujimura, Y. *J. Am. Chem. Soc.* **2003**, *125*, 8019.
(54) Sugawara, M.; Fujimura, Y. *J. Chem. Phys*. **1994**, *101*, 6586.
(55) Ohtsuki, Y.; Zhu, W.; Rabitz, H. *J. Chem. Phys*. **1999**, *110*, 9825.
(56) Ohtsuki, Y.; Nakagami, K.; Zhu, W.; Rabitz, H. *Chem. Phys*. **2003**, *287*, 197.
(57) Xu, R.; Yan, Y.; Ohtsuki, Y.; Fujimura, Y.; Rabitz, H. *J. Chem. Phys*. **2004**, *120*, 6600.
(58) Ohtsuki, Y.; Ohara, K.; Mayumi, A.; Nakagami, K.; Fujimura, Y. *Chem. Phys. Lett*. **2003**, *369*, 525.
(59) Sobolewski, A. L.; Domcke, W.; Dedonder-Lardeux, C.; Jouvet, C. *Phys. Chem. Chem. Phys*. **2002**, *4*, 1093.